Tracking of Scalpel Motions With an Inertial Measurement Unit System

Ernest Kabuye, Tess Hellebrekers, Justin Bobo, Nolen Keeys, Carmel Majidi, Jonathan Cagan, and Philip Leduc

***Abstract*—Surgical planning to visualize a complete procedure before surgical intervention, paired with the advanced surgical techniques of a surgeon, has been shown to improve surgical outcomes. Efforts to improve surgical planning have included tracking real-time surgeon movements via surgical instruments in a confined body cavity space in the human body to enhance specific techniques when performing minimally invasive surgery. In this work, a surgical tool tracking approach is presented that leverages small scale electronics to enable real-time position capture for use in iterative surgical planning. By integrating a lightweight 9 degree-of-freedom Inertial Measurement Unit (IMU), our system captures both spatial and temporal information of the surgical tool without requiring a direct line-of-sight. The IMU is printed on a flexible film and attached to and integrated with a surgical tool demonstrating its tracking capabilities. Data from the IMU is analyzed to determine the full range of motion during angular displacement for measurement and tracking. The results show an accuracy of 2.2^0, 2.9^0 and 3.1^0 of the full range of motion of the X (Yaw), Y (Roll) and Z (Pitch) Euler angle coordinate system respectively demonstrating the potential for surgical tool tracking measurement without the need for a direct line of sight and with future impact including flexible electronics and motion tracking. This work will be helpful in a diversity of fields including surgery, surgical training, biomaterials, and motion tracking.**

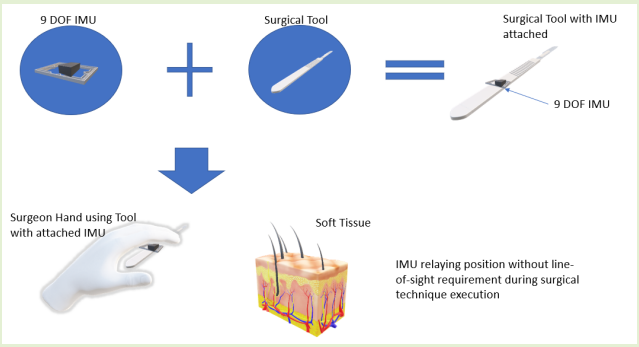

***Index Terms*—Small scale electronics, flexible electronics, surgical procedures, tool tracking, inertial measurement.**

I. Introduction

PRE-OPERATIVE surgical planning involves the use of computer aided imagery to super impose multiple layers of the anatomy to set defined surgical paths [1]. The dynamic status of these anatomical regions during surgical procedures means that real-time iterative surgical planning based on changing surgical tool locations to guarantee positive surgical outcomes and decrease surgical time is critical [2]. Further improvements in technology, using smaller scale visually based electronics in such surgery, have also provided the ability to create motion-tracking sensors that are integrated with surgical instruments to improve real time feedback for iteration of surgical operating and planning scenarios in these confined cavity spaces. However, these surgical tool tracking approaches all require a direct line of sight with bulky and expensive visual markers. Currently, to assist surgeons in tracking surgical tools while performing minimally invasive surgical procedures, commercially available [3] systems like the NDI Polaris Vega use a combination of visual active and passive markers [4]. These markers are visible impressions on surfaces strategically placed in an operating room and on the surgical tools, which enable the optical tracking of the surgical tools with respect to the target site tissue deformation [5] and rely on hand tracking for precision and accuracy [6]. This approach not only augments the user's surgical technique, but also ascertains a path for pre-surgical planning. Other commercial systems utilizing computer vision (CV) like the Procedicus MIST and the Reachin Laparoscopic Trainer have been designed to deploy additional haptic feedback [7], [8] to the intended user and help with fundamental surgical skills assessment [6] and motion analysis tracking with assistance from augmented reality. Despite all these features, as user preference is a target [9], these VR systems still require a direct line of sight to the target area for surgical training effectiveness.

A promising alternative to CV-based approaches involves the use of inertial measurement units (IMUs). This is because an IMU can be programmed to transmit motion tracking data without the need for a direct line of sight. Technological

Manuscript received November 12, 2021; accepted January 6, 2022. Date of publication January 21, 2022; date of current version February 28, 2022. This work was supported by the Office of Naval Research under Grant N00014-17-1-2566. The associate editor coordinating the review of this article and approving it for publication was Dr. Shanhong Xia. *(Corresponding author: Ernest Kabuye.)*

The authors are with the Department of Mechanical Engineering, Carnegie Mellon University, Pittsburgh, PA 15232 USA (e-mail: ekabuye@andrew.cmu.edu; cagan@cmu.edu; prl@cmu.edu).

Digital Object Identifier 10.1109/JSEN.2022.3145312

advances with robotic surgery [10], smart instruments[11] and flexible and stretchable electronics [12], [13] have brought about the use of IMUs in various applications [14]. IMUs measure a body's force, angular rate, and orientation through a combination of accelerometers, gyroscopes, and magnetometers. Wearable IMU devices integrated with electronics and optical biosensors can provide various real time data, from temperature to drug delivery [15]. In medical applications, IMUs have also been used to monitor and measure gait analysis in body joints [16], [17] as well as improvement in placement of class III [18] medical devices such as pedicle screws [19]. While promising for surgical applications, prior work is limited both in incorporating only 6 degree-of-freedom (DOF) IMUs, thereby limiting position accuracy, and physical incorporation and integration into small, and in particular hand-held, surgical tools.

Our work in this paper introduces a method for tracking a surgical instrument using a 9 DOF IMU, printed on a flexible circuit, that is directly attached to and integrated into a surgical tool, to provide real time motion tracking at higher accuracy, reducing dexterity interference, and a measurement profile of a proposed surgical path without the need for a direct line of sight. This advancement enables and provides the capability for an un-occluded pre-surgical and iterative surgical path plan.

II. Related Work and Motivation

A. Surgical Tool Tracking

During tissue resection, surgical procedures entail contact with tissues via dexterous tissue manipulation [20]. To provide a simulated feedback loop using augmented reality for accompanying systems, errors due to noise, latency, position or even orientation need to be minimized [21]. MEMS (micro-electrical mechanical system) have been designed to generate simulated feedback in the form of haptic transduction as input for robotic assisted minimally invasive surgery [22]. However, orientation error persists in these systems, and this increases user error, which negatively impacts surgical planning. In a challenging scenario [21], the user would experience between 0.9^0 to 4.7^0 angular error in orientation error when tracking distant (maximum distance of 61 m) objects while still being able to track the user's head with an InterSense IS-900 6 degree of freedom tracker. Here, a negative denotes a shift to the left-hand side of the real environment from projection of the augmented environment and is akin to having a user look left towards a target object placed in the front of their view. Additional work in video-based tracking of laparoscopic tools using the visible characteristic point of the tool [23] to determine tool position and orientation determined that for gesture analysis and an objective evaluation of surgical maneuvers, an overall volumetric accuracy of 2.89 mm root-mean-square (RMS) and 9.28 mm RMS [24] at a constant and a variable depth respectively is desired.

In other instances of surgical tool tracking, an optical approach is used through utilizing imagery of the cylindrical shape of a surgical instrument [25], along with a camera position that can be used to determine the position and orientation of an endoscopic instrument in an operating room. This approach localizes five degrees of freedom (i.e., two rotation angles around an access point, insertion depth, and rotation of the instrument around an axis). However, this method has accuracy limitations as well as registration errors [26]. This approach also can only be used for large-scale position tasks such as surgical navigation assistance tasks like proximity warnings and thus for augmented reality guidance in surgeries that require greater precision of 5μm such as workspace measurement or tele-mentoring, accurate tracking would be challenging [27]. To address the registration error, other systems have used head mounted displays that relay select real time data to the user [28]. These have been used in environments where the alignment of this imagery with the physical anatomy is feasible, but this approach provides a limited scope-of-view to the surgeon.

B. Inertial Measurement Unit Sensing

To provide improved tracking of surgical instruments in this field, advances using IMUs utilizing more than 6 DOF (Degree of Freedom), with each degree of freedom denoting an axis, have been proposed. These advances include algorithms that have been designed to measure and account for error estimation in measurements caused by magnetic distortions in the proximal field [29]. This error information is critical in establishing the accuracy of surgical tool tracking when these proposed systems are compared with commercially available surgical robotic systems. Commercially available systems like the Polaris Spectra and Vicra [30] employ optical tracking algorithms that specify an overall volumetric root-mean-square (RMS) distance accuracy of 0.25mm and an orientation error average of 0.362^0 for an active rigid body based on a combination of up to 12 markers, (with each marker providing 6 DOF, this comes to 72 DOF necessary for tracking). Other commercial systems like the Vive tracker, utilizing 6DOF, have been used to track body motion with IMU's to within 0.26^0 for the angular displacement and have thus been established as the benchmark for best performance [31].

C. Motivations of Research

The approach introduced in this work is motivated by the advancement of small-scale electronics, specifically, IMU's related to medical applications such as surgical path planning [32]. Despite the viability of commercial tracking systems, their more complex set up, requirement of a direct line-of-sight and the high cost make them challenging to use for surgical path planning implementation that is required for successful surgical outcomes. The flex PCBs, via the IMU enables a much tighter integration with surgical tools without a direct line-of-sight requirement.

Other advances in attempting to address the sensing deficiencies of a 9-DOF IMU through calibration [33] of the output and in combination with Extended Kalman Filters to improve its accuracy in measurement have been made [29]. To date, a majority of IMU's rely on only the accelerometer and gyroscope for precision tracking. By adding a magnetometer, the accuracy for the measurement of the tracking of surgical tools could be significantly improved. However,

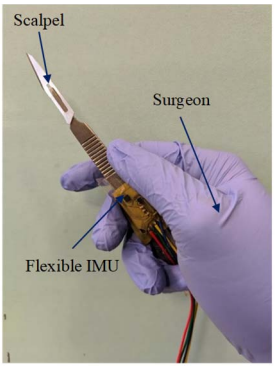

Fig. 1. A surgeon hand holding a scalpel with a flexible IMU attached to the center of the tool. The ending wires denote the power and signal transmission lines for setup.

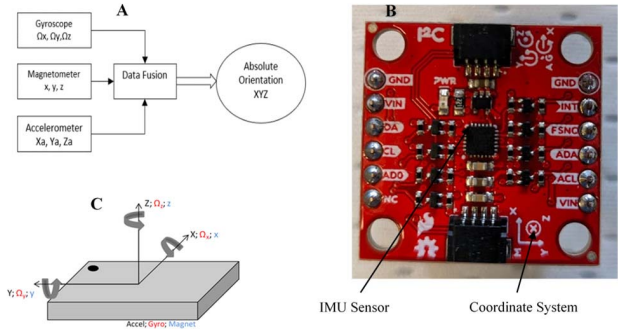

Fig. 2. **(A)** Data Fusion Schematic on the IMU showing the 9 DOF fused from each 3 axis from each sensor on the IMU board. **(B)** ICM 20948 IMU; **(C)** IMU Sensor coordinate system showing the axes provided form each of the three sensors namely the accelerometer, gyroscope, and magnetometer.

incorporating an IMU with an additional degree of freedom from the magnetometer could create faulty readings due to soft and hard iron distortions [34]. The former is related to objects that can influence the magnetic field around the IMU, and the latter is related to separate objects that create their own magnetic field that distorts other magnetic fields.

This paper integrates a 9 degree-of-freedom IMU in combination with a surgical tool as an approach for tracking tool motion in a confined cavity space and relaying this real time data for an iterative approach for surgical planning. *Fig. 1* displays a surgeon holding a surgical tool that has been fitted with a flexible IMU for real time tool tracking. A surgical path is defined for the surgeon to follow with their tool. The tool location is presented on the orientation display monitor in full view of the surgeon. The surgical path is then updated per this real time information to account for the tissue dynamics. The additional axis in the IMU not only improves measurement and location precision, but also helps address direct line-of-sight and head mounted display weight challenges without impeding any surgical technique guidelines. The approach is then tested to demonstrate a full range of motion with the proposed IMU combination.

III. Test Methodology

A. Inertial Measurement Unit

For surgical tool tracking, a 9-DOF IMU, InvenSense ICM20948, is used, which contains 3 internal triple-axis MEMS sensors. The first sensor is an accelerometer that measures rotation and translation through an output of electrical capacitance when placed under mechanical stress. The accelerometer contains capacitive plates internally that are attached to a mechanical spring that moves internally as acceleration forces act upon the sensor. The movement of the plates relative to each other causes a capacitive change, that allows the acceleration to be determined. The second sensor is a gyroscope that measures a body's relative position to the earth's gravitational field. It accomplishes this by measuring the angular velocity from the body's rotation around an axis and correlating that to a voltage to determine the position. The third sensor is a magnetometer that measures a body's proximity to the gravitational field. It accomplishes this by measuring the change in electrical current from the change in magnetic flux density around a body. The magnetic field affects the motion of the electrons, and this change can be used to determine the direction of the magnetic field. Each sensor (gyroscope, accelerometer, and magnetometer) provides data for a three-axis coordinate system for a total of 9 DOF that, when combined with a manufacturer's or application data fusion algorithm, from all three sensors by the onboard Digital Motion Processor (DMP), creates a single three axis (XYZ) absolute orientation coordinate system (*Fig. 2*). Given the dynamic nature of movement, the earth field has a significant magnetic inclination or dip that is geographically dependent. By using the gyroscope to estimate this position and account for this magnetic dip, the onboard DMP will then approximate the heading angle of the magnetometer using the pitch and roll measurements from the accelerometer and then output the final precise position through a motion fusion algorithm. Of note, the 9-DOF IMU provides the data to the algorithm, and any individualized algorithm can use the data to articulate a precise location.

This coordinate system defines the output data axis as X (yaw), Y (roll) and Z (pitch) and is derived from Tait-Bryan angles, also known as nautical angles or Euler angles [35] also primarily used in gait posture estimation and analysis [36].

B. Surgical Path Planning Setup

In a clinical setting, surgical tool placement in the center of the palm (*Fig. 1*) is not only done for ergonomics but also to ensure that the surgeon movements during minimally invasive surgery are not impeded as this is a position that is widely used when performing certain surgical techniques such as incision into cavity regions [6]. The proposed surgical tool tracking method would have a customized flexible IMU attached to the central pivot of the surgical tool versus being positioned on either end of the tool. This flexible IMU placement not only maintains the ergonomic attributes but also does not impede a surgical technique with a direct line of sight requirement. Calibration of the IMU to accurately track a surgical tool is then marked critical as this precise location after the calibration step is what will be used to iterate the pre-planned surgical path once surgery is engaged. With this surgical

technique position selected, it is mindful to note that despite dexterity of surgical techniques being considered subjective and unquantifiable, measurement of time taken to complete a surgical task correlate to positive surgical outcomes [37]. However, the focus in this paper is the surgical path chosen and it is a vertical path to simulate an incision into tissue.

C. IMU Setup and Calibration

An IMU sensor (InvenSense ICM20948) is programmed through an Arduino to provide output sensor data (*Fig. 2*) with a custom API built to filter out the noise at a 115200 baud sampling rate based on the manufacturer supplied sensitivity range for each of the different sensors. The data fusion from all three sensors (*Fig. 2*) provides data as a 3-D space absolute orientation X (Yaw), Y (Roll) and Z (Pitch) coordinate system.

To account for hard and soft iron distortions in the field as well as any variations/noise, the magnetometer has programmable digital filters that limit the range of measurement data to within the manufacturer's specification. The gyroscope and accelerometer sensors, similarly per the manufacturer's specification, have a 1x average filter that smoothed out the data during sampling.

The calibration is accomplished for each sensor on the board per recommended manufacturing specifications. To calibrate the accelerometer, the shorter side of the board with the black circle in *Fig. 2* is moved along the 3 axes in both directions and is maintained in that position for 5 seconds. The gyroscope is calibrated by moving the board for 5 seconds and letting it rest on the table for 5 seconds. The magnetometer is calibrated by moving the board in a figure-8 style motion for a total of 5 times.

The internal runtime and background calibration for the IMU ensures that optimal performance of the sensor data is maintained with each output of absolute orientation data point (X, Y, Z) by having a system (Sys) level wide reading next to it (*Fig. 3*). This will display a range from 0 (bad) to 3 (great) for the calibration confidence for each sensor: A - accelerometer, G – gyroscope, and M- magnetometer. This system (Sys) is a measure of the calibration confidence from data fusion for each data point as the measurement accuracy is made by the corresponding sensor.

D. Sensor Output

For the proposed tracking method, the IMU sensor provides a structured data set for absolute orientation that is obtained from the 9 degrees of freedom measurements. As one example in the case of a tumor biopsy where an incision is made to perform a biopsy [38], this tracking method is meant to simulate motion during the actual moment that the surgeon, following a path of least resistance with a surgical tool like a scalpel, makes physical contact with the compact tissue. At this point of contact, there is limited further lateral motion with respect to the surgeon holding the scalpel in hand and the change in absolute orientation is related to a pivot at the wrist to make a vertical incision into a tissue with the scalpel. Due to this technique, this scenario can be modeled and tracked with an absolute orientation system. Because of the small cavity of the body within which the surgeon must operate, the accuracy of knowing this precise location, which is then communicated to other systems used in surgical path navigation, is critical. The range for each absolute orientation axis (*Table I*) is the same as a Euler angle coordinate system for absolute orientation tracking.

TABLE I
DATA OUTPUT SCHEMATIC AND OPERATING RANGE FOR IMU

Orientation	Description	Angular displacement(deg)	Total motion
X	Yaw	0 to 360	360^0
Y	Roll	-90 to +90	180^0
Z	Pitch	+180 to -180	360^0

Sys	X	Y	Z
3	67.6	-40.58	15.66
3	67.73	-40.76	15.73
3	67.86	-40.95	15.79
3	67.99	-41.13	15.84
3	68.13	-41.3	15.9
3	68.25	-41.49	15.95
3	68.37	-41.68	16.04
3	68.46	-41.87	16.12
3	68.56	-42.05	16.22
3	68.66	-42.23	16.3
3	68.78	-42.42	16.36
3	68.91	-42.61	16.39
3	69.03	-42.8	16.43
3	69.15	-43	16.48

Fig. 3. Sample customized IMU sensor output data (Post Processing) showing an object whose gyroscope, accelerometer and magnetometer provide the system "great" calibration ("3"). Each column corresponds to the nautical axis X(Yaw), Y(Roll) and Z(Pitch).

MATLAB and C++ software on the Arduino are employed to analyze the output data from the customized IMU and are output using an Arduino MKRZERO board. For the analysis step, only data points whose system (Sys) calibration is verified (i.e., a value of 3) is plotted with the rest discarded *Fig. 3* shows a sample of this data output from absolute orientation tracking of a stationary object that has undergone full calibration prior to data gathering.

E. Data Analysis

For data analysis, overall volume RMS distance error is used to analyze the error after multiple runs. Data points from each run are compared with each other over time to determine the difference, $\varepsilon_{\mathrm{RMS}}$, between the measured positions, $\mathrm{r_m}$, and their corresponding reference position, $\mathrm{r_r}$, as $\varepsilon_i = r_{ri} - r_{m_i}$ for each data point, i. For this analysis, the first run is taken as the baseline run and the positions are obtained from their angular displacement, in degrees, based on the full range of motion

$$\varepsilon_{RMS} = \sqrt{\frac{1}{N}\sum_{i=1}^{N}(\varepsilon_i \cdot \varepsilon_i)}. \quad (1)$$

F. Manufacturing of Flexible Printed Circuit Devices

To ensure that the electronics are compatible with the contours of the surgical scalpel, the IMU and supporting

Fig. 4. **Top:** Printed Circuit Board Manufacturing Process. **Bottom Left (A)**: Schematic for flexible printed circuit board. **Bottom Right (B)**: Flexible IMU printed on film substrate with soldered wire touchpoints.

MEMS are populated on a flexible printed circuit board. The flexible PCB (fPCB) is manufactured by combining flexible materials with integrated circuit (IC) electronics to provide a thin and compliant construction with enhanced conformity.

The layout of the (fPCB) [39] is defined using Autodesk EAGLE PCB Design Software and fabricated (Fig. 4) using a wax printer (8570D Xerox ColorQube, Xerox), which selectively deposits a masking ink onto a single-side copper Kapton laminate (∼50 μm Kapton, ∼35 μm copper, 25 μm polyimide film). Hydrogen Peroxide, hydrochloric acid, and water are then mixed (2:1:1) to etch the sacrificial copper layer that is exposed by the printed pattern. Additional manual etching of the printed wax ink by a small scratch brush leaves a conductive copper circuit trace (Fig. 4). Finally, rigid IC (integrated circuit) chips are soldered to the circuit.

G. Angular Rotation Setup

To test the response of the IMU, the system is attached to a horizontal platform (*Fig. 5*) to examine the angular motion by rotation around a primary axis. The horizontal base platform is mounted on a Stepper motor (NEMA-17 size-200 steps/rev, 12V 350mA) via a vertical rod 4.5 inches in length and a coupler to transmit the torque from the motor to the base platform via a 9V power supply. The stepper motor is programmed via an Arduino IDE for complete clockwise revolutions in micro steps at controlled speeds from 5 to 60 RPM. Dexterous tissue manipulation is approximated at speeds of 5 RPM with a target determination for a maximum speed of 60 RPM.

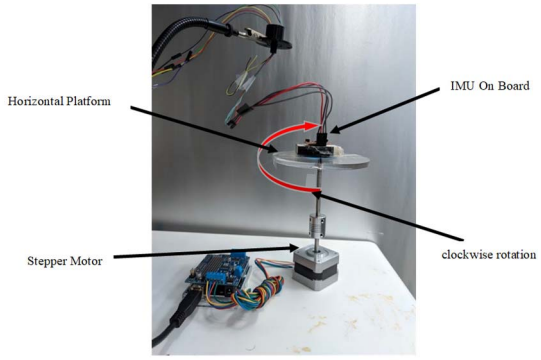

Fig. 5. IMU circuit board on a test bed platform designed to rotate the base platform around one primary axis at a time.

The run test on the test platform first implements the internal calibration of the axes corresponding to the three different sensors. To provide clockwise continuous motion, a stepper motor is controlled via an Arduino UNO R3 board for 30 continuous clockwise revolutions. This clockwise motion is accomplished through the rotation of a primary axis while fixing the secondary and tertiary axes for capturing data specific to the rotational ranges outlined in *Table I*. An analysis of the points generated throughout the runs enable the determination of the range of values obtained by plotting the data points whose system wide level calibration is 3 ("great calibration"). This is repeated over multiple speeds defined as low (5 rpm), medium (15 rpm), and high (60 rpm). The run test is then utilized for each of the other remaining axes by changing the primary axis of rotation while having the other two axes fixed.

Continuous motion of the test system shows a linear saw tooth response along the profile of its expected values in that axis. The continuous motion manifests as a saw tooth profile because the angular measurement goes back to the beginning counter after passing the maximum measurement. *Fig. 6* is a representative example of this continuous saw-tooth motion, specifically in the Y axis (Roll), for 5 runs of the rotation. Each angled line is a linear increase as the IMU rotates around the Y axis (Roll) in a Euler angle coordinate system. Each angled line represents one run from start to finish. The y-axis of the graph is measured angular displacement (motion) in degrees and the x axis is time in seconds.

IV. Results

A. Angular Displacement Results

The absolute orientation versus normalized time in seconds (Fig. 13) displays the motion profile over time during each run. The angular displacement in degrees is on the y-axis with the normalized time duration on the x-axis with speeds of low (5rpm), medium (15rpm) and high (60rpm) marked as solid lines, diamond squares and plus sign designation, respectively.

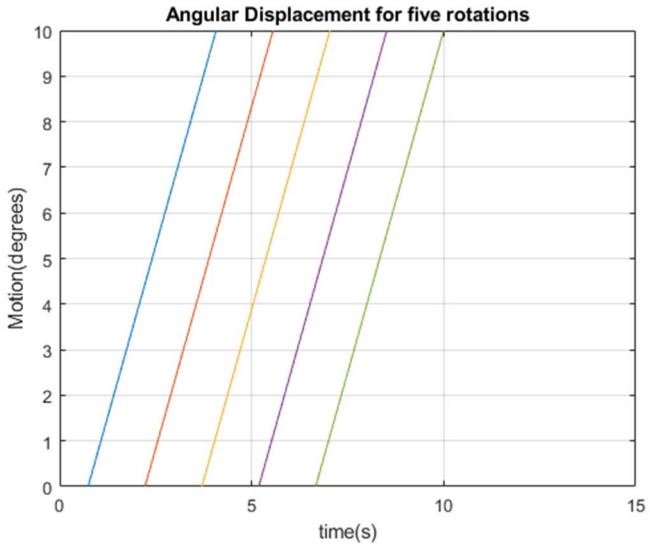

Fig. 6. Angular displacement for five rotations in the Y(Roll) axis as the primary axis at a slow speed of 0.5 RPM. The angular displacement of this axis is from -90^0 to 90^0 normalized over a scale of 0-10.

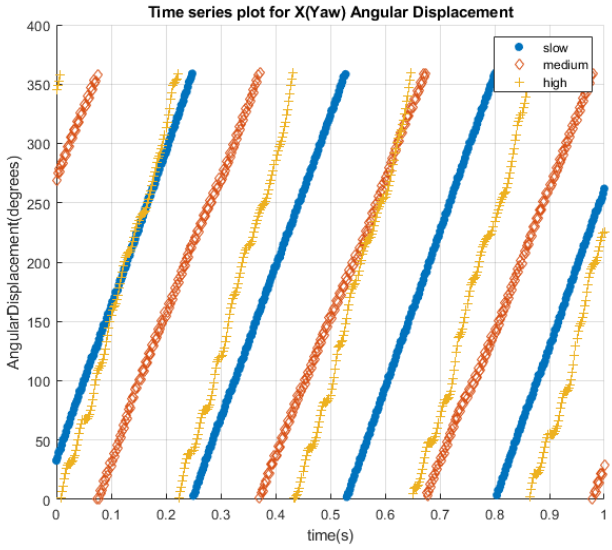

Fig. 7. Time series plots for the X (Yaw) axis is shown above. Each angled line in the Yaw represents a fully tracked angular motion throughout the range for that axis. Speeds for low, medium, and high rotation are shown.

A full range of motion showing the angular displacement is obtained for all the runs through all speeds

Fig. 7 is the approximately linear increase when angular displacement is tracked, and the output is the X (Yaw) axis. On close examination, the serrated profile in the data is more prevalent at slow and medium speeds than at higher speeds where a smooth transition is displayed.

Similarly, for the Y (Roll) axis in Fig. 8, the angular displacement profile shows the peaks of each run. However, the full range of measurement for the angular displacement falls within a much tighter band of -80 to 80 degrees as opposed to -90 to 90 degrees. There is a loss in scaling for measurements in this absolute orientation axis. This loss in scaling can either be accounted for during the calibration by introducing data points with weaker calibration confidence (up

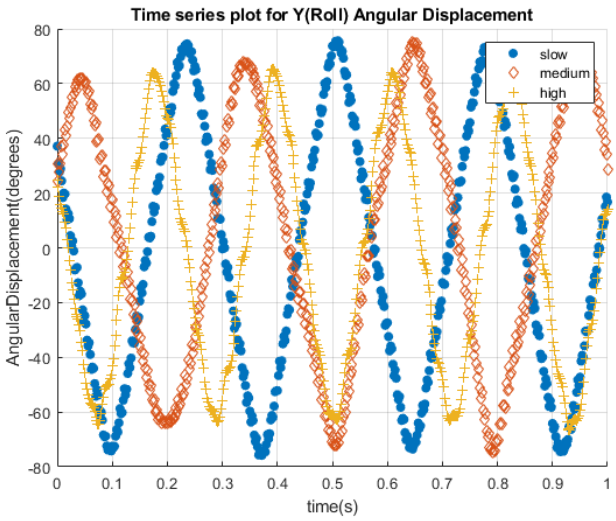

Fig. 8. Time series plots for the Y(Roll) axis is shown above. Each sine wave is a fully tracked angular rotation. Speeds for low, medium, and high rotation are shown.

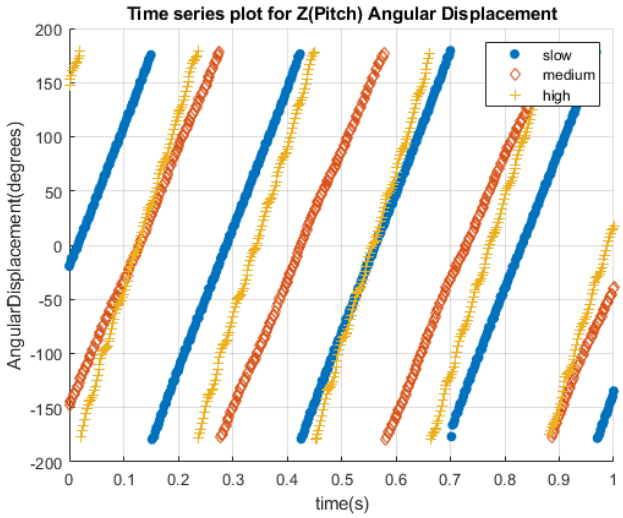

Fig. 9. Time series plots for the Z(Pitch) axis is shown above. Each angled line in the Yaw represents a fully tracked angular motion throughout the range for that axis. Speeds for low, medium, and high rotation are shown.

to Sys level 2) or by rescaling it to -90 to 90 degrees. Fig. 9 is the angular displacement of the output for the Z (pitch) axis has a linear decrease over time and has the expected output in the range of -180 to 180 degrees. Overall, the IMU can repeatably capture and output absolute orientation measurement around all three axes in a Euler angle coordinate system.

B. Signal Comparison

Rotational motion in all three Euler axis directions is then further analyzed. The motion is imposed over 30 runs at medium speed (15rpm) for the same amount of time for each absolute orientation axis *(Table II)*. After the time synchronization, the root-mean-square difference for each axis is calculated to examine the difference between each run. These 30 runs are overlaid on each other to visualize and quantify

TABLE II
SIGNAL COMPARISON ALL ABSOLUTE ORIENTATION AXES

Axis	*Root Mean Square Difference between Runs(degrees)*	*%Error*
X (Yaw)	*2.2*	*1.2*
Y (Roll)	*2.9*	*3.2*
Z (Pitch)	*3.1*	*1.7*

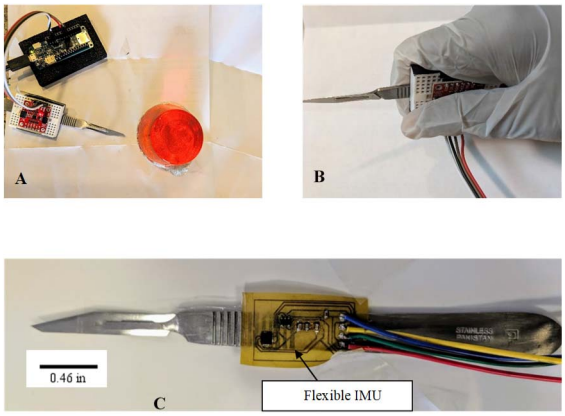

Fig. 10. Top left (A): Printed circuit board IMU on a surgical scalpel prior to cutting a gelatin-based muscle mimetic tissue substrate; Top right (B): The printed circuit board IMU attached to surgical scalpel in a hand; Bottom (C); Flexible IMU attached to surgical scalpel at the center of tool instrument.

any differences in their profiles for each absolute orientation axis.

To account for the gyroscope noise in the setup and IMU board, per the manufacturers' instructions, a 0.05 general tolerance is assigned to ascertain that all values are within 5% of each measurement variable across the three orientation data plots. In addition, a 1%-time difference is included for proper signal alignment per the ramp time difference as the test for each run. This helps to synchronize the time between the start of the runs. The most significant difference appears to occur at the transition points of the measurement, specifically at the end of the scale of each orientation data axis measurement. The differences that occur at this transition point will likely increase the RMS differences (*Table II*) in the data signal output throughout the runs for each axis. The signal comparison shows the RMS falls outside the $0.26^0 - 0.36^0$ range for tracking surgical tools using commercially available equipment utilizing optical trackers and acceptable percent error for each absolute orientation axis.

C. IMU Integration With Scalpel on Gelatin-Based Mimetic Tissue System

After analyzing the motion tracking of the IMU on the test bed platform, the IMU based system is attached to a surgical scalpel (*Fig. 10*) via the fPCB. The purpose of mounting the circuit to the scalpel is to simulate the clinical conditions necessary for the proposed surgical application. Tracking of the tool will allow real time iterative surgical planning to occur.

The motion of this assembly is tracked during its initial contact with, and via an incision cut on, a gelatin based

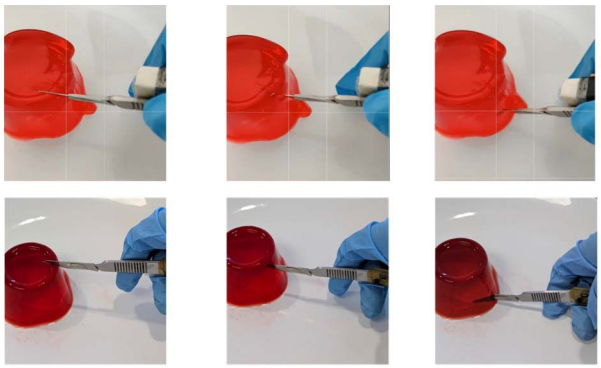

Fig. 11. The images (left to right) display the progression of one incision cut into the gelatin muscle substrate as the scalpel moves from top to bottom. **Top**: surgical scalpel attached with IMU at its center pivot. **Bottom:** surgical scalpel attached with **flexible** IMU at its center pivot.

biomimetic substrate (*Fig. 11*) based on a pre-planned surgical vertical path. The gelatin is a type of hydrogel that can be used as 3D tissue scaffolds due to tissue-like mechanical properties such as elasticity, stiffness and geometry and thus have been used as engineered tissue to simulate muscle-like structures [40]. Hydrogels have further been used to 3D bio print aortic valves [41] while maintaining mechanical properties such as ultimate strength and peak strain and maintaining the tensile biomechanics comparable to actual muscle tissue. The IMU is attached to the center of the scalpel as an approximate pivot point for tracking absolute orientation data. Three incisions are made in a positive and negative (up and down vertical) motions in the Z axis (Pitch) Euler axis into the gelatin muscle tissue substrate. These three incisions are made in new locations each time. The movement of the sensor translates to the angular displacement in terms of the pitch (Z axis) for the measurement. It is important to note that mechanical response of the tissue is not accounted for here, but in the future that would help close the loop required to provide a defined surgical path based on tool location, mechanical response of the tissue, etc. in this cavity space.

In addition, the flexible IMU is then wrapped around the scalpel with the overall scalpel position similar to the printed circuit board (*Fig. 11*) to simulate tissue response during scalpel motion for three incisions into the gelatin using a proposed application setup of the flexible IMU.

The motion of the flexible IMU attached to the surgical scalpel in Fig. 12 shows three different peaks signifying the angular displacement of the scalpel each time the scalpel enters and leaves the gelatin muscle substrate. This motion is expected to be reflected only in the Z-axis (Pitch). The motion profile for all three axes during the three incisions is shown in Fig. 13. In this motion tracking of all three orientation Euler axes, the Z-axis (Pitch) shows a change in angular displacement consistent with the three incisions with each incision peak signifying that respective travel. The angular displacement in the Y axis (Roll) and the X axis (Yaw) is expected to be relatively linear during the three incision peaks into the gelatin muscle substrate as the only movement made by an experienced surgeon would happen in the Z axis (Pitch). However, due to the lack of surgical experience of the

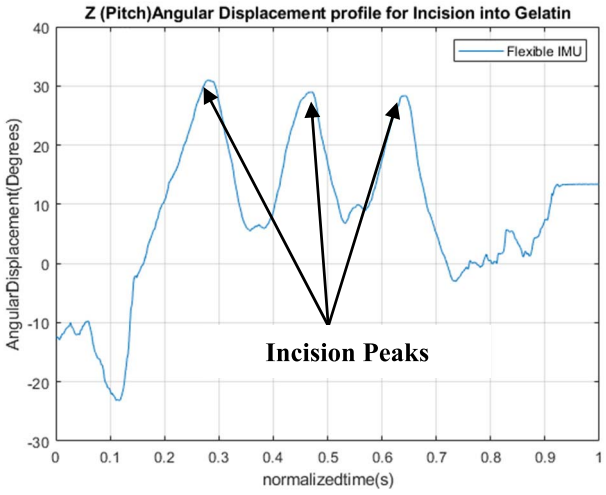

Fig. 12. Z (Pitch) Angular Displacement Profile for Incision into Gelatin.

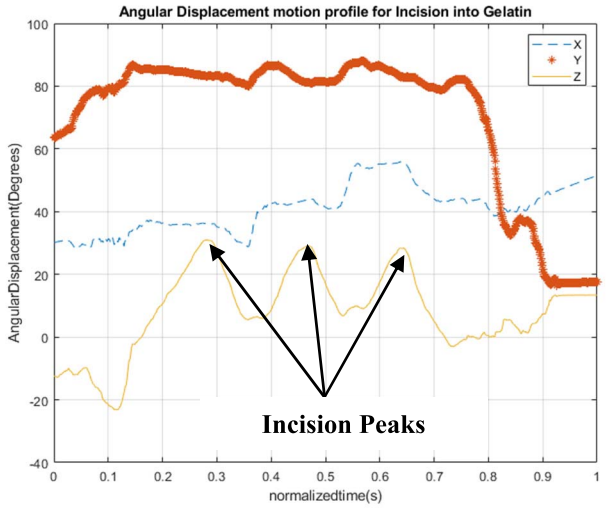

Fig. 13. Angular Displacement motion profile for incision into Gelatin muscle substrate for all three Euler orientation axes. The peaks are shown in the Z(Pitch) and relative flatline movement is shown for X(Yaw) and Y(Roll) concurrently.

experimenter, limited angular displacement occurs during the incision into the gelatin muscle substrate, as indicated by the non-flat profile of the tracked angular displacement in the X axis (Yaw) and Y axis (roll), during the three peaks associated with the incisions found in the Z axis (Pitch) in Fig. 13.

It is also important to note that for the proposed experimental setup, there is no tracking of the lateral linear motion of the scalpel and only the absolute orientation of an object at its pivot is tracked. This setup represents the actual surgical incision cuts made manually in the field. The absolute orientation picked for surgical tool tracking is reflective of the type of iterative surgical planning that is hard to predict and would require further analysis as a base comparison between the proposed approach of a flexible IMU attached to a surgical tool and an industrial tracking method that utilizes a commercial product with optical tracking capabilities as a benchmark. Furthermore, the decision to take only calibration data points, with a Sys level 3 for analysis, made in pre- and post-processing of the data output for the IMU, enabled a consistent output for the three axes with the data not being affected by magnetic distortion.

V. Conclusion

The ability of a 9DOF IMU to track measurement motion related to a surgical tool without requiring a direct line of sight has been demonstrated for absolute orientation tracking in this paper.

Real time surgical tool locations are necessary to help close the feedback loop of a pre-surgical planned path to generate new surgical paths as the surgical procedure is carried out. Current approaches that rely on optical trackers to track the user and the surgical tools in this environment through a direct line of sight can hinder a full understanding of surgical techniques as the user would have to accommodate the constraint. A 9 DOF IMU is integrated onto our test platform to demonstrate its utility in a full angular motion measurement representative of absolute orientation by engaging in one of its axes at a time to track the motion. The IMU and data analysis allows us to obtain absolute orientation data for a tracked surgical instrument. This approach is then used to move and track a scalpel, attached with a customized flexible IMU, through a gelatin based biomimetic substrate when a series of incisions is made in the absolute orientation frame. The capability of tracking as a flexible IMU film could be useful to integrate with other minimally invasive surgical approaches like gloves to provide additional autonomy with surgical planning. In future work, the volume root-mean-square angular displacement is currently outside the desired accuracy and further refinement of the approach would be beneficial. In addition, this setup is intentionally not placed next to equipment that generates its own magnetic field leading to specific hard iron distortion, which may cause challenges in other scenarios. Effects of this distortion are partially addressed and minimized not only through calibration but also through selective filtering of the data. In a clinical setting, equipment that causes extreme hard iron distortion is normally separated and operated independently. The future work of this application will eliminate all these ferromagnetic distortions on the measurement data captured.

Since actual surgeries have varying surgical skillsets, and, in this paper, we introduce technology for surgical planning and training, a surgical plan of a manual vertical incision into tissue that is tested demonstrates functionality of the proposed application. Future research will study the use of the technology in human subject experimentation and will also expand work into establishing the accuracy and proficiency of the user in relation to these surgical techniques as the current method in the paper is focused on task execution.

This approach can be applied to other applications, such as tracking a surgical tool along a defined and known path to determine real time error and its effects on proper surgical planning. Furthermore, the ability to link to motion when interacting with other tissue substrates with different mechanical properties will allow for integration with system analysis and augmented reality approaches. Overall, our work will be of interest to a diversity of fields including medicine, engineering,

and computer science. The use of a 9 DOF IMU, and in particular a flexible one, to accurately track measurement profiles of surgical tools without need for a direct line of sight is a novel addition in this regard.

REFERENCES

[1] C. Charbonnier *et al.*, "ArthroPlanner: A surgical planning solution for acromioplasty," *Int. J. Comput. Assist. Radiol. Surg.*, vol. 13, no. 12, pp. 2009–2019, Dec. 2018, doi: 10.1007/s11548-018-1707-9.

[2] J. Castro-Nnez, J. M. Shelton, S. Snyder, and J. Sickels, "Virtual surgical planning for the management of severe atrophic mandible fractures," *Craniomaxillofacial Trauma Reconstruction*, vol. 11, no. 2, pp. 150–156, Jun. 2018, doi: 10.1055/s-0037-1601865.

[3] J. E. Lang *et al.*, "Robotic systems in orthopaedic surgery," *J. Bone Joint Surg. Brit.*, vol. 93, no. 10, pp. 1296–1299, Oct. 2011, doi: 10.1302/0301-620X.93B10.27418.

[4] P. Dutkiewicz, M. Kieáczewski, and M. Kowalski, "Visual tracking of surgical tools for laparoscopic surgery," in *Proc. 4th Int. Workshop Robot. Motion Control*, 2004, pp. 23–28, doi: 10.1109/romoco.2004.240569.

[5] Y. Han, Y. Rabin, and L. B. Kara, "Soft tissue deformation tracking by means of an optimized fiducial marker layout with application to cancer tumors," *Int. J. Comput. Assist. Radiol. Surg.*, vol. 15, no. 2, pp. 225–237, Feb. 2020, doi: 10.1007/s11548-019-02075-0.

[6] S. Shaharan, D. M. Ryan, and P. C. Neary, "Motion tracking system in surgical training," in *Motion Tracking and Gesture Recognition*. London, U.K.: InTech, 2017, doi: 10.5772/intechopen.68850.

[7] O. A. J. Van Der Meijden and M. P. Schijven, "The value of haptic feedback in conventional and robot-assisted minimal invasive surgery and virtual reality training: A current review," *Surg. Endoscopy*, vol. 23, no. 6, pp. 1180–1190, 2009, doi: 10.1007/s00464-008-0298-x.

[8] S. P. Lee, T. C. T. Qui, S. C. Loy, and W. R. Pensyl, "Haptic interaction in augmented reality," in *Proc. 17th ACM Int. Conf. Multimedia (MM)*, 2009, p. 975, doi: 10.1145/1631272.1631475.

[9] N. Tovares, P. Boatwright, and J. Cagan, "Experiential conjoint analysis: An experience-based method for eliciting, capturing, and modeling consumer preference," *J. Mech. Design*, vol. 136, no. 10, Oct. 2014, Art. no. 101404, doi: 10.1115/1.4027985.

[10] M. Diana and J. Marescaux, "Robotic surgery," *Brit. J. Surg.*, vol. 102, no. 2, pp. e15–e28, Jan. 2015, doi: 10.1002/bjs.9711.

[11] M. R. Mahfouz, G. To, and M. J. Kuhn, "Smart instruments: Wireless technology invades the operating room," in *Proc. IEEE Topical Conf. Biomed. Wireless Technol., Netw., Sens. Syst., BioWireleSS*, 2012, pp. 33–36, doi: 10.1109/BioWireless.2012.6172743.

[12] N. Naserifar, P. R. LeDuc, and G. K. Fedder, "Drop casting of stiffness gradients for chip integration into stretchable substrates," *J. Micromech. Microeng.*, vol. 27, no. 4, Apr. 2017, Art. no. 045018, doi: 10.1088/1361-6439/aa63af.

[13] N. Naserifar, P. R. LeDuc, and G. K. Fedder, "Material gradients in stretchable substrates toward integrated electronic functionality," *Adv. Mater.*, vol. 28, no. 18, pp. 3584–3591, May 2016, doi: 10.1002/adma.201505818.

[14] N. Ahmad, R. A. R. Ghazilla, N. M. Khairi, and V. Kasi, "Reviews on various inertial measurement unit (IMU) sensor applications," *Int. J. Signal Process. Syst.*, vol. 4, pp. 256–262, Jan. 2013, doi: 10.12720/ijsps.1.2.256-262.

[15] A. K. Yetisen, J. L. Martinez-Hurtado, B. Ünal, A. Khademhosseini, and H. Butt, "Wearables in medicine," *Adv. Mater.*, vol. 30, no. 33, Aug. 2018, Art. no. 1706910, doi: 10.1002/adma.201706910.

[16] S. Bakhshi, M. H. Mahoor, and B. S. Davidson, "Development of a body joint angle measurement system using IMU sensors," in *Proc. Annu. Int. Conf. Eng. Med. Biol. Soc.*, Aug. 2011, pp. 6923–6926, doi: 10.1109/IEMBS.2011.6091743.

[17] T. Seel, J. Raisch, and T. Schauer, "IMU-based joint angle measurement for gait analysis," *Sensors*, vol. 14, no. 4, pp. 6891–6909, 2014, doi: 10.3390/s140406891.

[18] R. E. Ferner and J. K. Aronson, "Medical devices: Classification and analysis of faults leading to harms," *Drug Saf.*, vol. 43, no. 2, pp. 95–102, Feb. 2020, doi: 10.1007/S40264-019-00879-2.

[19] S. Baba *et al.*, "Use of an inertial measurement unit sensor in pedicle screw placement improves trajectory accuracy," *PLoS ONE*, vol. 15, no. 11, Nov. 2020, Art. no. e0242512, doi: 10.1371/journal.pone.0242512.

[20] D. Bouget, M. Allan, D. Stoyanov, and P. Jannin, "Vision-based and marker-less surgical tool detection and tracking: A review of the literature," *Med. Image Anal.*, vol. 35, pp. 633–654, Jan. 2017, doi: 10.1016/j.media.2016.09.003.

[21] M. A. Livingston and Z. Ai, "The effect of registration error on tracking distant augmented objects," in *Proc. 7th IEEE/ACM Int. Symp. Mixed Augmented Reality*, Sep. 2008, pp. 77–86, doi: 10.1109/ISMAR.2008.4637329.

[22] M. Hamidullah, A. T. H. Lin, B. Han, and Y. J. Yoon, "A sensorized surgical needle with miniaturized MEMS tri-axial force sensor for robotic assisted minimally invasive surgery," in *Proc. IEEE 14th Electron. Packag. Technol. Conf.*, Oct. 2012, pp. 57–60, doi: 10.1109/EPTC.2012.6507051.

[23] R. Dockter, R. Sweet, and T. Kowalewski, "A fast, low-cost, computer vision approach for tracking surgical tools," in *Proc. IEEE Int. Conf. Intell. Robot. Syst.*, Oct. 2014, pp. 1984–1989, doi: 10.1109/IROS.2014.6942826.

[24] A. M. Cano, F. Gayá, P. Lamata, P. Sánchez-González, and E. J. Gómez, "Laparoscopic tool tracking method for augmented reality surgical applications," in *Biomedical Simulation* (Lecture Notes in Computer Science), vol. 5104. Berlin, Germany: Springer, 2008, pp. 191–196, doi: 10.1007/978-3-540-70521-5_21.

[25] O. Tonet, T. U. Ramesh, G. Megali, and P. Dario, "Tracking endoscopic instruments without localizer: Image analysis-based approach," *Stud. Health Technol. Informat.*, vol. 119, no. 1, pp. 544–549, 2006, doi: 10.3109/10929080701210782.

[26] D. Guha, N. M. Alotaibi, N. Nguyen, S. Gupta, C. McFaul, and V. X. D. Yang, "Augmented reality in neurosurgery: A review of current concepts and emerging applications," *Can. J. Neurol. Sci.*, vol. 44, no. 3, pp. 235–245, May 2017, doi: 10.1017/cjn.2016.443.

[27] L. H. Eadie, A. M. Seifalian, and B. R. Davidson, "Telemedicine in surgery," *J. Brit. Surg.*, vol. 90, no. 6, pp. 647–658, Jun. 2003, doi: 10.1002/bjs.4168.

[28] X. Chen *et al.*, "Development of a surgical navigation system based on augmented reality using an optical see-through head-mounted display," *J. Biomed. Inform.*, vol. 55, pp. 124–131, Jun. 2015, doi: 10.1016/j.jbi.2015.04.003.

[29] H. Ren and P. Kazanzides, "Investigation of attitude tracking using an integrated inertial and magnetic navigation system for hand-held surgical instruments," *IEEE/ASME Trans. Mechatronics*, vol. 17, no. 2, pp. 210–217, Apr. 2012, doi: 10.1109/TMECH.2010.2095504.

[30] A. Andrew, D. David, and J. Donald, "Accuracy assessment and interpretation for optical tracking systems," *Proc. SPIE Med. Imag. Vis., Image-Guided Procedures, Display*, vol. 5367, pp. 421–432, May 2004.

[31] J. Thomas, M. Bordeleau, and M. Applegate, "Agreement analysis between Vive and Vicon tracking systems to monitor lumbar postural changes," *Ann. Phys. Rehabil. Med.*, vol. 61, p. e481, Jul. 2018, doi: 10.1016/j.rehab.2018.05.1124.

[32] H. Ren, D. Rank, M. Merdes, J. Stallkamp, and P. Kazanzides, "Multisensor data fusion in an integrated tracking system for endoscopic surgery," *IEEE Trans. Inf. Technol. Biomed.*, vol. 16, no. 1, pp. 106–111, Jan. 2012, doi: 10.1109/TITB.2011.2164088.

[33] N. Yadav and C. Bleakley, "Fast calibration of a 9-DOF IMU using a 3 DOF position tracker and a semi-random motion sequence," *Measurement*, vol. 90, pp. 192–198, Aug. 2016, doi: 10.1016/j.measurement.2016.04.066.

[34] J. C. K. Chow, "Statistical sensor fusion of a 9-DOF MEMS IMU for indoor navigation," Tech. Rep., 2017, doi: 10.5194/isprs-archives-XLII-2-W7-333-2017.

[35] C. Ma, M. Z. Q. Chen, J. Lam, and K. C. Cheung, "A novel body frame based approach to aerospacecraft attitude tracking," *ISA Trans.*, vol. 70, pp. 228–237, Sep. 2017, doi: 10.1016/j.isatra.2017.05.014.

[36] R. Takeda, S. Tadano, A. Natorigawa, M. Todoh, and S. Yoshinari, "Gait posture estimation using wearable acceleration and gyro sensors," *J. Biomechanics*, vol. 42, no. 15, pp. 2486–2494, Nov. 2009, doi: 10.1016/j.jbiomech.2009.07.016.

[37] T. D. Jackson, J. J. Wannares, R. T. Lancaster, D. W. Rattner, and M. M. Hutter, "Does speed matter? The impact of operative time on outcome in laparoscopic surgery," *Surg. Endoscopy*, vol. 25, no. 7, pp. 2288–2295, Jul. 2011, doi: 10.1007/s00464-010-1550-8.

[38] C. P. Karakousis and C. P. Karakousis, "Surgical technique in cancer surgery," in *Atlas Operative Procedures Surgical Oncology*. New York, NY, USA: Springer, 2015, pp. 1–11, doi: 10.1007/978-1-4939-1634-4_1.

[39] M. D. Bartlett, E. J. Markvicka, and C. Majidi, "Rapid fabrication of soft, multilayered electronics for wearable biomonitoring," *Adv. Funct. Mater.*, vol. 26, no. 46, pp. 8496–8504, 2016, doi: 10.1002/adfm.201602733.

[40] V. Hosseini *et al.*, "Engineered contractile skeletal muscle tissue on a microgrooved methacrylated gelatin substrate," *Tissue Eng. A*, vol. 18, nos. 23–24, pp. 2453–2465, 2012, doi: 10.1089/ten.tea.2012.0181.

[41] B. Duan, L. A. Hockaday, K. H. Kang, and J. T. Butcher, "3D bioprinting of heterogeneous aortic valve conduits with alginate/gelatin hydrogels," *J. Biomed. Mater. Res. A*, vol. 101A, no. 5, pp. 1255–1264, May 2013, doi: 10.1002/jbm.a.34420.

Ernest Kabuye received the B.S. degree from Northeastern University in 2011 and the M.S. degree from Tufts University in 2016. He is pursuing the Ph.D. degree in mechanical engineering with Carnegie Mellon University, as a GEM Fellow. He has extensive work experience in the medical device field designing products for Becton Dickinson and Smith & Nephew. His research focuses on technological advances within the healthcare field.

Tess Hellebrekers, photograph and biography not available at the time of publication.

Justin Bobo, photograph and biography not available at the time of publication.

Nolen Keeys, photograph and biography not available at the time of publication.

Carmel Majidi, photograph and biography not available at the time of publication.

Jonathan Cagan received the B.S. and M.S. degrees from the University of Rochester in 1983 and 1985, respectively, and the Ph.D. degree from the University of California at Berkeley in 1990.

He has been on the faculty with Carnegie Mellon University (CMU) since 1990 and was promoted to a Professor in 1999, where he currently serves as the Interim Head of Mechanical Engineering and previously served as the Interim Dean for the College of Engineering in 2019, having served as the Associate Dean for four years prior. He co-founded the Integrated Innovation Institute for interdisciplinary design education at CMU, including its three M.S. programs in product, service, and software innovation and entrepreneurship, and a start-up accelerator in Silicon Valley. He also served as the Co-Faculty Director of the Swartz Center for Entrepreneurship, CMU, where he is the George Tallman and Florence Barrett Ladd Professor in Engineering with the Department of Mechanical Engineering, with courtesy appointment in Design. He has nearly 300 peer-reviewed publications and multiple patents. His research focuses on engineering design automation and methods, merging AI, machine learning, and optimization methods with cognitive science problem solving. His recent efforts include computer–human teaming, generative design, and biomechanical systems design and diagnostics. Both his design methods and computer-based design research have been applied in a variety of industries.

Dr. Cagan is a Fellow of the American Society of Mechanical Engineers. He was a recipient of the Engineering College's Outstanding Research Award, the University's Robert A. Doherty Award for Sustained Contributions to Excellence in Education, the ASME Design Theory and Methodology Award, the Design Automation Award, and the Ruth and Joel Spira Outstanding Design Educator Award. He is a registered Professional Engineer.

Philip Leduc received the B.S. and M.S. degrees in 1993 and 1995, respectively, and the Ph.D. degree from Johns Hopkins University in 2009. He was a Postdoctoral Fellow with the Boston Children's Hospital and the Harvard Medical School. He is the William J. Brown Professor with the Mechanical Engineering Department, Carnegie Mellon University, with appointments in Biomedical Engineering, Computational Biology, and Biological Sciences. He has filed numerous patents, has started companies, and has consulted for a diversity of companies. He has also been involved with many philanthropic organizations, including raising money for non-profit organizations and mission trips to Africa and Armenia. During his career, he has published articles in many journals, including *Proceedings of the National Academy of Sciences*, *Nature Nanotechnology*, *PLoS ONE*, *JACS*, *Applied Physics Letters*, *Methods in Cell Biology*, *Advanced Materials*, *Nano Letters*, *Nature Protocols*, and *Nature*. He is a Fellow of the Biomedical Engineering Society, the American Society of Mechanical Engineers, and the American Institute for Medical and Biological Engineering. He has received the National Science Foundation CAREER Award and the Beckman Foundation Young Investigators Award, while also being selected as a Faculty Member for the Sloan Foundation Minority Ph.D. Program. He has also been funded by other organizations, including the Bill & Melinda Gates Foundation, the Office of Naval Research, the Department of Energy, the National Institute of Health, and the Keck Foundation. He has given seminars across the world, including South Africa, India, and Brazil. He has been on and helped organize many scientific meetings, including for the National Academy of Engineering, the National Academy of Sciences, the Institute of Medicine, and the United States Congress, and being elected to the Science Advisory Council of the Beckman Foundation, and the Board of Directors for the Biomedical Engineering Society and the American Institute for Medical and Biological Engineering.